PCCP

Accepted Manuscript

ROYAL SOCIETY OF CHEMISTRY

www.rsc.org/pccp

The H + $HeH^+ \rightarrow$ He + H_2^+ reaction from the ultra-cold regime to the three-body breakup: exact quantum mechanical integral cross sections and rate constants.

Dario De Fazio*

Istituto di Struttura della Materia - C.N.R., 00016 Roma, Italy

March 15, 2014

Abstract

In this work, we present a quantum mechanical scattering study of the title reaction from 1 mK to 2000K. Total integral cross sections and thermal rate constants are compared with previous theoretical and experimental data and with simpler theoretical models to understand the range of validity of the approximations used in the previous studies. The obtained quantum reactive observables have been found to be nearly insensitive to the roto-vibrational energy of the reactants at high temperatures. More sensitive to the reactant's roto-vibrational energy are the data in the cold and ultra-cold regimes. The implications of the new data presented here in the early universe scenario is also discussed and analyzed.

1 Introduction

The prototypical chemical reaction H + $HeH^+ \rightarrow$ He + H_2^+ plays a special role in astrophysics. In some sense it can be considered the 'mother' of chemistry, being arguably the first active chemical reaction to take part in our universe [1]. In fact, according to the standard Big-Bang theory, from the primordial nucleosynthesis the nucleus of very few elements has been generated [2]. At those times, most of the matter was electrons, protons and alpha particle with some relevant abundance of their isotopes (nuclei of deuterium and ^{3}He),

*defazio.dario@yahoo.it

plus some traces of lithium. The universe was essentially a charged plasma with radiation and matter in thermodynamical equilibrium and the matter was practically fully ionized. Because of the adiabatic expansion, radiation and matter started to be decoupled with the temperature of the matter quickly decreasing. When the matter temperature was low enough, the atoms started to recombine by radiative association forming the first neutral atoms. Because of its largest ionization potential, the He atom was the first neutral atom to be formed, according to the reaction:

$$\mathrm{He}^+ + \mathrm{e} \rightarrow \mathrm{He} + \nu \tag{1}$$

When this happened, it could encounter one of the many protons available, and form by radiative association enhanced by the strong cosmic background radiation [3] the first molecular system, namely the HeH^+ molecule:

$$\mathrm{He} + \mathrm{H}^+ + \nu_{\mathrm{back}} \rightarrow \mathrm{HeH}^+ + \nu' \tag{2}$$

When the universe was cooled enough to permit also the recombination of hydrogen atoms, the fast reaction with HeH^+ could be competitive with the radiative dissociation induced by the cosmic background radiation, leading first to the molecular hydrogen cation:

$$\mathrm{H} + \mathrm{HeH}^+ \rightarrow \mathrm{He} + \mathrm{H}_2^+ \tag{3}$$

and then to H_2, after encountering another neutral hydrogen atom:

$$\mathrm{H} + \mathrm{H}_2^+ \rightarrow \mathrm{H}^+ + \mathrm{H}_2 \tag{4}$$

The formation of molecular species in the primordial universe is extremely important, because roto-vibrational quantum states became available to participate in the cooling process, permitting the dissipation of the radiative energy and balancing the increase of the gravitational energy during the collapse of the first cosmological objects. The characterization of the cooling process is highly relevant for astronomers, because it can give reliable information about how and when the first cosmological objects came to being. The high dipole moment of HeH^+ (about 1.66 Debye) and its high number of vibrational bound states (12 [4]) make this cation a possible important coolant especially in the early period of the recombination era when the H atom was not formed yet. The rate of the H+ HeH^+ reaction is therefore doubly important in the cooling process: (i),

because the depletion rate controls the HeH^+ abundance. (ii), because it is the key step in one of the main mechanisms of hydrogen molecule formation in the primordial plasma [5], strongly affecting the hydrogen abundance in the red shift range 150-300. The temperature dependence of the rate of this simple exothermic process is therefore crucial in order to establish the molecular abundances and the early universe evolution [6]. The temperatures required in the cosmological models change by several orders of magnitude, from about ten to several thousand Kelvin, with particular relevance for the lowest range.

Regarding the low temperature regime, HeH^+ is also a possible candidate to be cooled in ionic traps, where important recent advances [7] have been achieved in the control of the kinetic ion energy in cold and ultra-cold conditions [8]. Also, the existence of HeH^+ in many different astrophysical enviroments (planetary nebulae, dense molecular clouds, white dwarfs) has been discussed in several papers (see e.g. [9, 10]). Because of so many astro-chemical applications, accurate reaction data are required in the full collision energy range, from the ultra-cold regime to the three-body breakup and beyond.

From the theoretical point of view, the title reaction is also a theoretical prototype of exothermic ion molecule processes, a class of chemical reactions very common in the interstellar medium, so that an accurate characterization of its dynamics and of the reaction mechanism is highly relevant to extrapolate typical features to be included in the astrophysical models and to estimate the reliability of the mandatory approximations required to describe the more complex ion-molecule processes of the astro-chemical networks.

Notwithstanding its relevance in atrophysics and cosmology, the $H + HeH^+$ reaction has been still relatively little investigated. To our knowledge, only quasi-classical trajectories studies have been recently performed [11, 12] focalizing on the stereodynamics of the system and of its isotopic variants. Also recently, a few quantum mechanical calculations have been reported [13, 14, 15], but the large number of approximations introduced to solve the nuclear motion problem could significantly affect relevant aspects of the dynamics and further 'exact' quantum studied are required to check their reliability. With the exception of Ref. [15], most of the studies were restricted to the ground reactant's roto-vibrational level, while reactant's excited state-to-state data are required for more advanced plasma models [5, 16], and probably also for ion trap experiments simulations.

From the experimental point of view, few and very old measurements [17, 18] at high collision energies are the only data available. Because of this lack of information, these data were extrapolated at low temperatures [19] and included in the modeling of the early universe evolution [20, 21]. These measurements were

also corroborated by the calculations of Ref. [13], but a completely different behaviour of the integral cross sections (ics) was found in the low collision energy range (below about 10 meV), a range highly relevant under the primordial universe conditions. The new molecular abundances obtained with these new theoretical data [13], have shown important effects in the low red shift region (5-70), supporting the need of accurate data for this reaction to obtain a realistic astrophysical description of the evolution of the early universe.

With the motivations described above we present here an 'exact' quantum dynamics study of the title reaction from ultra-cold collision energy to the three-body dissociation breakup. In Sec. 2 we briefly summarize the dynamical algorithm (Sec. 2.1) and some details are given on the potential energy surfaces (Sec. 2.2) employed in the calculations. In Sec. 3 we present integral cross sections (Secs. 3.1 and 3.2) and rate constants results (Sec. 3.3), giving also a comparison with experimental data, previous theoretical calculations, and other simpler theoretical models. Finally, in Sec. 4 we discuss the possible relevance of the obtained results in the early universe scenario, and give some indications regarding further theoretical developments, that could be useful to obtain a more accurate description of the kinetic data.

2 Computational Methods

2.1 Quantum reactive scattering calculations

Time independent quantum reactive scattering calculations have been performed using a modified and parallelized version [4, 22] of the ABC code of Manolopoulos and co-workers [23]. The ABC program uses a coupled channel hyperspherical coordinate method to calculate the quantum mechanical scattering matrix. Within the program, the set of coupled hyperradial equations is solved using a log derivative propagator [24]. In the modified code, an Enhanced Renormalized Numerov (ERN) method [25] is applied to propagate the hyperradial wavefunctions from ρ_{n-1} to ρ_n with n ranging from 1 to $n_{max} - 1$:

$$\mathbf{R}_n = \mathbf{Q}_n - \mathbf{O}_{n,n-1}\mathbf{R}_{n-1}^{-1}\mathbf{O}_{n-1,n} \tag{5}$$

In eq. (5), $\mathbf{O}_{n,n-1}$ is the overlap matrix between the hyperspherical eigenfunctions calculated at ρ_n and ρ_{n-1}, $\mathbf{R}_n$ is the ratio matrix [25] of the hyperradial functions, and $\mathbf{Q}_n$ is the diagonal matrix of the Thorlacius and

Cooper propagator [26], with diagonal entries given by:

$$[\mathbf{Q}_n]_i = \begin{cases} 2\cos\frac{d\sqrt{[2\mu(\epsilon_i(\rho_n)-E)]}}{\hbar} & \text{for} \quad \epsilon_i(\rho_n) > E \\ 2\cosh\frac{d\sqrt{[2\mu|(\epsilon_i(\rho_n)-E)|]}}{\hbar} & \text{for} \quad \epsilon_i(\rho_n) < E \end{cases} \tag{6}$$

where μ is the three body hyperspherical reduced mass, d is the size of the hyperradial sector, $\hbar$ is the Planck constant divided by 2π, $\epsilon_i(\rho_n)$ is the i-th eigenvalue of the internal hyperspherical Hamiltonian calculated at ρ_n and E is the total energy of the system. At $n = n_{max} - 1$, the logarithmic derivative matrix was recovered and used to finish the propagation with the logarithmic derivative propagator as in the original code, leaving unchanged the final matching equations.

The implementation of this modification has been essential to obtain highly converged $S-$matrix elements also in the ultra cold regime, while keeping low the number of the hyperradial sectors. To demonstrate the improvement of the new propagator, in Fig. 1 we show the values of the total ics for zero total angular momentum J, obtained with our code and with the original ABC programme as a function of the number of the hyperradial sectors (m_{max}) employed in the calculation. Three collision energies (reported on the panels) in the ultra-cold (panel (a)), cold (panel(b)) and low (panel (c)) collision energy regimes are selected. To obtain smooth behaviours all the others input parameters were set to give a convergence within 0.1% (see the caption for numerical values). Each panel also reports by dot-dashed lines, the range of ics with differences within 1 $\%$ of accuracy with respect to the asymptotic value. The first point emerging from the figure is that the ERN method converges much faster than the logarithmic derivative, by about one order of magnitude in the cold and ultra-cold energy regimes. Also we note that in these regimes the convergence of ERN is always variational while the logarithmic derivative always converges from below. Comparing the behaviours in the three panels, we can note (see e.g. the ics values in the neighbourhood of the dot-dashed lines) that while in the logarithmic derivative case the convergence is energy dependent, for the ERN the percent error is constant with the collision energy. This is a large advantage for the cold and ultra-cold regimes where previous calculations performed with the ABC code (see e.g. [27]) required very fine hyperradial grid to get converged results. However, the performance improvement of the ERN method is gradually attenuated at higher energies, reaching about a factor 3 at collision energy near to 1 meV (panel (c)), where opposite convergence behaviours are found. However, the convergence speed in the logarithmic derivative case is much lower increasing the collision energy so that a large number of hypersectors is still required to get high

accuracy results (within 0.1%).

To obtain convergent ABC parameters to be used in the 'production runs', the range of total energies covered by the calculations has been divided in eight macro-sectors defined in Table I: the convergence of the ics for the first four reactants rotational states has been studied for 20 evenly spaced energies in each sub-range. The values required to give convergence better than 1% for all the reactants rotational states studied are given in Table I. The same $S-$matrices obtained in the 'production runs' for collision energies above 2 meV have been used to obtain ics for different rotational reactants states (at different translational collision energies). However, the particular parameter values required in threshold dynamics studies (see below), require specific calculations at the opening of the energy threshold of excited reactants rotational levels. The convergence parameters used in these $j-$specific calculations are also given in Table I.

As we can note by comparison with Table II of Ref. [4], the convergent parameters above 2 meV are essentially the same of the ones previously reported for the He + H_2^+ reaction. However, in this case total ics converge slightly better because of the higher number of roto-vibrational states summed for the present exothermic reaction that average differences among the state-to-state results. Although only total ics are presented in this work, we prefer to keep unchanged the parameters in these ranges to make it possible to obtain with the same $S-$matrices state-to-state ics and differential cross sections of the same level of accuracy. Particular care has been devoted to study the convergent behaviour in the cold and ultra-cold collision energy ranges because of the large differences found with previous studies [14, 15] of this reaction. However as shown in the Table, no relevant differences have been found with the convergence parameteres of the low energy range (2.2-43.8 meV), except for the expected increasing of the maximum hyperradius ($rmax$) and the decreasing of the number of the partial waves required $Jmax$ and of their projection in the body-fix frame $kmax$. Comparing the threshold values of the parameters for different initial rotational states we can note a slight increase of $Jmax$ and $kmax$ with j indicating some delay to reach the Wigner threshold law behaviour and a more relevant role of the Coriolis coupling for describing the threshold dynamics of excited reactants rotational states (see Sec. 3.2). We also note that although some increasing of $rmax$ is required to obtain convergent ics in the cold and ultra-cold regimes, the values are rather contained (30 a.u.) in contradiction with the data reported for other three-body reactions (see e.g. Ref. [27]). Actually we find the calculations very cheap in these collision energy ranges from the computational point of view. However it is hard to generalize this result at other three-body reactions and PESs, also considering that the PES

employed does not contain the correct long-range multipole behaviour [28] in the analytical function used to fit the $ab-initio$ data (see Sec. 2.2).

To increase the efficiency also of the high energy calculations, where a large number of partial waves is involved (see Table I), the code has been amply parallelized (for details of the parallel strategies implemented, see [22] and [29]). For this light mass and symmetric (see below) application, requiring contained dimensions of the basis set employed (about 2500 in the worst case), a hybrid OpenMP/MPI implementation without communications among the computational cores has been sufficient to get results in a few hours (20 at the worst) of elapsed time on the IBM Blue Gene/Q supercomputer machine for each energy range studied. The speed-up of the OpenMP part of the code is for this parallel implementation around 10. The calculations exploit the symmetry of the PES with respect to the hydrogen exchange performing independent calculations for $ortho-$ and $para-$ symmetry of the products. In particular, He + H_2^+ $S-$matrix elements at a given total energy, have been calculated and transposed to give the ics of the inverse reaction as required by the principle of microscopic reversibility. The $ortho-$ and $para-$ ics obtained are divided by two (to take into account the reduction of the product levels available) and summed. We have numerically checked the implementation reproducing all the numerical digits obtained by A + BC calculations not implementing the exchange symmetry. Operating in this way, we were able to reduce the basis set dimension (N) employed of about a factor 2 and the computational cost ($\propto N^3$) of an additional factor 4. Finally, the cross sections have been opportunely post-antisymmetrized [30, 31] by multiplying $ortho-$ and $para-$ ics for the respective Fermi-Dirac statistical weights to take into account the indistiguishability of the two hydrogen atoms.

2.2 The Potential Energy Surface

The studies of the HeH_2^+ system have a long history and several electronic Potential Energy Surfaces (PESs) suitable for dynamical calculations of the title reaction have been published in the literature. Initially, the most used PES has been that of Joseph and Sathyamurthy [32], obtained fitting by a Sorbie-Murrel functional a set of 596 *ab-initio* energies [33] at the Multi Configuration Self Consistent Field level of theory. Later, this set of energies has been used in Ref. [34] to obtain an alternative analytical fit. The accuracy of the quantum chemistry calculations was estimated to be within the root-mean-square deviation of the analytical fits obtained (around to 50 meV).

Significant improvement in the description of the intermolecular interaction was achieved in Ref. [35]

where 1727 *ab-initio* energies were evaluated using the Multi Reference Configuration Interaction (MRCI) method with an extended basis set (the correlation-consistent polarized valence cc-p V5Z of Dunning [36]). An original feature of this work was that the internuclear geometries where the quantum chemistry calculations were performed, were selected over an evenly spaced grid in hyperspherical coordinates, instead of a grid in internuclear distances as usual. In particular, many points were taken along the hyperspherical ridge of the reaction (the hyperradial line of separation between the valleys of reactants and products), and in the neighborhood of other critical points of the PES, which were expected to be more sensitive to the reaction dynamics. From this set of *ab-initio* energies, a large subset (1487) of geometries were selected mainly on an energy based criterium for the generation of the analytical PESs. The fits were made using a many-body expansion [34]. Three PESs with different root-mean-square (16, 13 and 12 meV) deviations were generated using three different degrees of the polynomials for the three body term (M = 6, 10 and 12 respectively) in order to test the sensitivity of the reaction dynamics [37].

To further investigate the relevance of the correlation energy in the electronic structure calculations, the same set of configurations has been later used in a Full-Configuration Interaction (Full CI) calculation [38]. These points were fitted using again the functional form of [34], obtaining PESs with root-mean-square deviations lower than that of the PESs of Ref. [35] (6 and 14 meV for M = 8 and 6 respectively). However, to reduce the computational effort a basis set of lower extension (namely a Dunning cc-p VQZ) was employed. All the energy points (1511 geometries) below the triatomic dissociation energy were fitted, optimizing simultaneously all coefficients and directly implementing the exchange symmetry in the functional, exploiting the updating of the version of the codes used [39, 40]. In addition, new more accurate diatomic curves were also generated and used in the fitting procedure to increase the accuracy of the global PES. To test the effect of these improvements in PES generation and to permit a rigorous comparison with the Full CI PESs, MRCI calculations with the same basis set used in Ref. [35] were repeated and used to generate the analytical fits with similar root-mean-square-deviations (7 and 14 meV for M = 8 and 6 respectively) as the ones obtained with the Full CI energies.

In Ref. [4] several aspects of the quantum chemistry studies of Refs. [35, 38] have been critically revised by performing new complete basis set *ab-initio* calculations for selected internuclear geometries as well as time-independent quantum scattering calculations of the He + H_2^+ reaction in an extended interval of energies, permitting a stringent experimental comparison of the dynamics of several vibro-rotational states

of the reactants. The comparison of the roto-vibrational frequencies of the diatomic fragments with the experimental data and with the new higher accuracy diatomic fits, has shown significant improvements in the diatomic curves of Ref. [38] with respect to the ones used in Ref. [35], especially for the higher roto-vibrational states of the HeH^+ ion. The analysis of the three-body quantum chemistry calculations performed indicates that the extension of the basis set is more important than the higher level of treatment of the correlation energy, so that the set of the MRCI *ab-initio* energies are to be considered more accurate than the Full CI ones. However, the reaction dynamics of the He + H_2^+ reaction was shown to be rather insensitive to the specific PES used, with the theoretical results reproducing reasonably well the global behavior of the experiments for the first four reactants vibrational states with all the PESs used. In particular, no differences at the scale of the experiments have been found among the results employing different fits of Ref. [38]. Only when H_2^+ is in the ground and in the first excited vibrational levels, significant differences can be detected with a clearly better agreement of the simulations employing the PESs of Ref. [35]. However, the strong dependence of the reaction yields to the reactants rotational quantum number of these specific vibrational states and the recognized low reactants rotational resolution of the experimental data [41, 42], casts doubts on the reliability of the experimental test.

Waiting for a new experiment able to shed light on the PESs questions of this important benchmark system, we use here in order to investigate the H + HeH^+ reaction mainly one of the PESs of Ref. [38], namely the M=6 fit to the MRCI *ab-initio* energies called hereafter RMRCI6 PES. The main reason of this particular choice is that previous dynamical studies [13, 14, 15] have been performed with this PES and we use it to permit an unambiguous comparison among the results. However, some preliminary calculations have been performed also with the other fits available to test the reliability of the main conclusions of the work. A subroutine of the PES used and the outcome of the dynamical calculations presented (j=0 total ics and rate constants), are supplied in the supplementary material [43] for benchmark purpose.

3 Results and Discussion

3.1 Integral Cross Sections

In Fig.2 total integral cross sections (ics)

$$\sigma_{vj} = \sum_{v'j'} \sigma_{vj,v'j'} \tag{7}$$

where

$$\sigma_{vj,v'j'} = \frac{\hbar^2 \pi g_s}{2\mu_{A-BC} E_{coll}(2j+1)} \sum_J (2J+1) \sum_{KK'} |S^J_{vjK,v'j'K'}|^2 \tag{8}$$

are presented for the ground reactants roto-vibrational state of the title reaction at collision energies up to 0.8 eV on a linear energy scale. In Eq.(8) v, j and K (v', j' and K') are the vibrational, rotational and helicity reactants (products) quantum numbers respectively, $S^J_{vjK,v'j'K'}$ are symmetry adapted $S-$matrix elements [23], g_s is the post-antisymmetrization factor [31] taking the values 3/2 (1/2) for j' odd (even) indipendently by the reactants quantum numbers, while μ_{A-BC} is the two-body reduced mass of the reactants. The sum in Eq.(7) is over all the open product vibro-rotational states v', j'. The figure also reports the previous results used in the astro-chemical simulations of the early universe evolution [13, 20, 21]. As anticipated in the introduction, most of these cosmologic models have used the Linder extrapolation [19] to fit the Rutheford experimental data [18], both reported in the figure with the relative error bars. Also we report in the same figure the Langevin capture theory ics [44]

$$ics_{lang} = \sqrt{\frac{\pi\alpha}{2\epsilon_0 E_{coll}}} \tag{9}$$

found to overestimate the experimental data by about a factor two. In Eq.(9) α is the dipole polarizabilility of the incoming atom and ϵ_0 is the vacuum electric constant. Dashed violet line are the results of Ref. [13]. As discussed in the Introduction, these results agree enough well with the experimental measurements and especially with the Linder extrapolation, except in the very low collision energy range hidden by the energy linear scale used in Fig. 2. We can note that our results disagree with the theoretical results presented in Ref. [13], expecially at the higher energies reported, although the same PES was employed in the calculations (see Sec. 3.2). This is presumably to be attributed to the well documented large relevance of the Coriolis

coupling in resonance dominated reaction [45], in particular in this specific system (see e.g. Refs. [35, 46]), coupling ignored in the calculation of Ref. [13]. A numerical confirmation has been obtained by setting to zero the $kmax$ parameter to test the relevance of the Coriolis coupling, obtaining ics (not reported here) underestimated of about a factor two in the high collision energy range. Also poor is the comparison of our results with the experimental data and with the Linder fit. A much better agreement is obtained with the Langevin capture theory ics especially in the high collision energy range, where the ics presented is found to satisfactorily approach the capture theory curve.

The significant discrepancies with the experimental data could cast doubts on the reliability of the specific PES employed. However, preliminary calculations with the other PESs of Refs. [35, 38] (not reported here) have shown very small differences of the ics values in the range of collision energy of the experimental data suggesting that the discrepancies are nearly insensitive to the PES used. Nevertheless, important differences can be observed in the low collision energy range (under about 100 meV) where the ics behaviour is strongly influenced by the fit used, confirming the well known sensitivity of the low energy dynamics to the details of the PES employed. Another possible source of discrepancies between experimental and theoretical data could be an insufficient reactants roto-vibrational resolution in the experiment of Ref. [18]. We note, in fact that no comments are reported in Ref. [18] on the rotational purity of the reactants beams. To check this aspect, in Fig.3 we report integral cross sections for the first three reactants rotational states of the HeH^+ cation, in the same collision energy range of Fig. 2. In the figure, our results are compared to the ones of Ref. [15]. We note that in the present results, the rotational effects is very small especially in the high collision energy range, where the different curves are practically indistinguishable. This result appears relevant in applied models, where often the ground state approximation is adopted because often few state-to-state dynamical data are available in the literature. A larger rotational effect is shown in the data of Ref. [15] in the same positive direction as our results. A similar behaviour is presented for the vibrational effect where the ics (not shown) are rather insensitive to the reactants vibrational energy in the experimental energy range. However, larger vibrational effects have been found in the low energy range (under 200 meV) where the maxima of the ics becomes lower increasing the vibrational quantum number and the ics become nearly independent of the reactants translational collision energy.

From the results shown in this section we must conclude that the reason of the large discrepancies between theoretical and experimental data probably comes from uncertainties in the calibration of the absolute

values of the experimental data. In fact we can note that the experimental results reproduce very well the translational collision energy trend of the theoretical data. However, a rescaling of the meauserements it is required to match with them. In order to show this, experimental data rescaled by a factor of 2.358 are also reported in Fig. 2.

3.2 The cold and ultra-cold regimes

As discussed in the Introduction and in Ref. [15], the title reaction is a possible candidate system to be studied in ion-moleculae traps, so that a study of the rotational effect of this reaction at low and ultra-low collision energies can be of interest for future experiments in this direction. Also, as will be shown in the next subsection, the ics in the low collision energy range are relevant for an accurate description of the early universe evolution.

In Fig. 4 the ics for the first three rotational states in the range 0.1-100 meV are reported in a log-log plot in order to emphasize the low energy behaviour. The obtained results are compared to the ones published in Ref. [15]. Strong resonance features are evident for the ground rotational state of the reactants in the range of collision energies between 10 and 100 meV. For higher rotational states the maxima of the ics slightly shift at higher collision energies and the resonance features gradually disappear. At lower collision energy the reactivity rapidly decreases for all the rotational states presented. Around 0.1 meV the ground rotational state reactivity is about three times the ones of j=2 and about one order of magnitude larger than for j=1. This behaviour is in evident disagreement with the results published in Ref. [15], where a small dependence with the collision energy was found for j=1 and 2 in the cold energy range. Nevertheless, a very good agreement is found for the ground rotational state in the range of collision energies 0.1-10 meV. As will be shown in the next subsection this lead to a good agreement of the rate constants of Ref. [13] under 100 K, a range of temperature very important for astrochemistry applications. Considering the analysis of the results reported in Ref. [15], the disagreement for j larger than zero results is presumably due to the higher relevance for rotational excited ics of the Coriolis coupling (see Table I): to neglect it drastically overestimates the reactivity of the K=0 component, leading to an inaccurate ics energy behaviour in the cold energy range.

The resonance features are more evident in the vibrationally resolved ics, shown on a linear scale in Fig.5. We note that an inversion of the vibrational product populations in the low and high energy range

suggests a change of the reaction mechanism in the two different regimes. In the low energy range higher vibrational products are more populated while, as the collision energy increases, the vibrational distibution becomes gradually colder. The resonance features are localized essentially in the range 10-100 meV, mostly localized near the two extremes of the range, producing a nearly double maximum in the convoluted excitation functions. More theoretical studies, as the ones presented in Refs. [47, 48], are necessary in order to clarify the physical origin of this intriguing resonance behaviour. Additional insight on the reactive mechanism can be also obtained by the analysis of the differential cross sections [49, 50], a study that we plan to do in the next future. In Fig. 5 we also compare results with and without post-antisymmetrization (see Sec. 2.2) to show the effect of the nuclear spin statistic on the total ics. As is shown in the figure, it is very small for total ics (and for rate constants) in the high energy range so that neglect it leads to an error of just a few (2-3) percent on the reactive observables here presented. However, this effect is relevant comparing state-to-state observables to the experiments [31] producing a characteristic saw-toothed behaviour in the product rotational distributions. We note here, that some effect (although small) can also to be detected in the total ics resonance pattern, suggesting that the resonance complex have a configuration near to the product as also supported by the geometry of the main potential well of the system [38].

Particularly interesting is the search of resonance features in the ultra-cold regime because of the possibility [51] to tune them with electric and magnetic fields to form triatomic stable structures. Fig. 6 shows the ultra-cold behaviour of the ics in a log-log plot. The ics exhibit a flat minimum around 0.1 meV. At lower collision energy, the ics start to increase, smoothly reaching the Wigner's threshold law limit behaviour [52]

$$ics_{wig} = \frac{4\pi\beta}{k} \tag{10}$$

around 0.001 meV. In Eq.(10) β is the imaginary part of the scattering lenght [53] and $k = \sqrt{2\mu_{A-BC}E_{coll}}/\hbar$ is the reactants wave number. A fit by Eq.(10) of the ics in the collision energy range $10^{-5} - 10^{-4}$ meV yields the imaginary scattering value β = 3.554 10^{-2} a.u. No resonance features are found in the neighbourhood of the reactivity threshold. This result disagree with that of Ref. [14] (reported as an indigo dashed line in the figure) where a strong virtual state effect [52] had been found. We have extensively searched for some resonance feature in this energy range, checking all the parameters of our calculations and increasing the energy resolution, but no feature was found. Therefore we must conclude that this effect is an artifact of the calculation of Ref. [14], probably coming from uncertainties introduced by the absorbing potential technique

employed. We note that not only to the virtual state feature but also the background scattering disagrees with our calculation in the ultracold energy range.

3.3 Rate Constants

The initial state specific rate constant k_{vj} at the temperature T can be calculated directly by a Boltzmann averaging of the total integral cross sections σ_{vj} of Eq.(7):

$$k_{vj}(T) = \sqrt{\frac{8}{\pi\mu_{A-BC}(k_BT)^3}} \int_0^\infty E_{coll}\sigma_{vj}e^{-E_{coll}/k_BT}dE_{coll} \tag{11}$$

where k_B is the Boltzmann constant. Thermal rate constants can be obtained by a weighted sum of the state specific ones of (11):

$$k(T) \;=\; \sum_{v}^{v_{max}} \sum_{j}^{j_{max}} w_{vj}(T)k_{vj}(T) \tag{12}$$

where the normalized weights $w_{vj}(T)$ take into account the relative population of each initial state at the specific temperature:

$$w_{vj}(T) \;=\; (2j+1)e^{-E_{vj}/k_BT} / \sum_{\tilde{v}}^{v_{max}} \sum_{\tilde{j}}^{j_{max}} (2\tilde{j}+1)e^{-E_{\tilde{v}\tilde{j}}/k_BT}. \tag{13}$$

In eq. (13) E_{vj} is the roto-vibrational energy of the entrance channel diatomic level.

As an alternative route, thermal rate constants can be extracted directly from the reaction probabilities without calculating explicitly the integral cross sections. In this formulation the thermal rates are obtained by a single integral

$$k(T) \;=\; \frac{1}{hQ_{int}Q_t} \int N(E)e^{-E/k_BT}dE. \tag{14}$$

over the cumulative reactive probabilities $N(E)$ summed over the total angular momentum J:

$$N(E) = \sum_{J}^{J_{max}} (2J+1) \sum_{vjK} \sum_{v'j'K'} g_s|S^J_{vjK,v'j'K'}|^2 \tag{15}$$

where E is the total energy and the sums in Eq. (15) are over all the open reactants and product channels. We note here, that to fullfill Eq.(14) the knowledge of the full reactive block of the $S-$matrix is required.

In (14), Q_{int} is the coupled roto-vibrational partition function for HeH^+ and Q_t is the relative translational atom-molecule partition function per unit volume:

$$Q_t = \frac{(2\pi\mu_{A-BC}k_BT)^{3/2}}{h^3} \tag{16}$$

The two methods (Eqs.(12) and (14)) are of course analytically equivalent if v_{max} and j_{max} are set to be the quantum numbers of the highest open channel of the reactants. However in most of the applications the ground state appromixation is invoked and v_{max} and j_{max} are taken as 0. This corresponds to assume that the reactivity is independent from the vibro-rotational energy of the reactants. However one of the advantages of using a time-independent method is that the full reactive $S-$matrix, required in Eq. (15), is the standard output of the calculations, so that the ground state approximation can be directly assessed.

In Table II rate constants calculated by Eqs.(12) and (14) are reported in the range 1 mK-2000 K and compared to the results of Table 2 of Ref. [13]. The first column gives the results of the ground state approximation, the second the results using v_{max}=0 and j_{max}=5, and the third the rates calculated with Eq. (15). The numbers are shown in Figure 7 in a log-log plot, similarly to [13] to visualize the global behaviours. The figure, demonstrates that the ground state approximation is in this case excellent in the full range of the investigated temperatures. Table II shows that the largest deviation from the 'exact' rate of Eq. (14) is less than 7% around 800 K. It is remarkable considering that at this temperature j=0 is about 6 % of the reactants and that at 2000 K it is only 2 %. The rates have practically quantitative accuracy (within 1 %) if j_{max} is taken to be 5. This result is of course due to the small rotational and vibrational effects discussed in Sec. 3.1 (see Fig. 3).

Another important feature shown in the Figure is that the rates published in Ref. [13] are rather accurate (within about 5 %) in the range 5-70 K, notwithstanding the large deviations discussed in Sec. 3.1 (see Fig. 2). This happens because of the large relevance in this range of temperatures, of the low energy behaviour of the j=0 ics in good agreement with the calculations of Ref. [13] (see first panel of Fig. 4). The discrepancies of course increase at higher T (near a factor two in the range of highest temperatures), but still remain inside the error bar of the experiment [17] at room temperature. At higher T the rates seems to tend toward the Langevin constant value of 2.088 $10^{-9}cm^{-3}sec^{-1}$, although at 2000 K they are still about 20% lower. To show the details of the high temperature range, the rates are plotted in Figure 8 on a linear-linear scale. An interesting detail emerging from the figure, is that the $k(T)$ of Eq. (14) have a flat maximum around to

1850 K that is not shown in the calculations performed with Eq.(12). It is due to the lower reactivity of the excited vibrational states at low collision energies (see Sec. 3.1) that at high temperature, where reactants excited vibrational levels are significantly populated, compensates and cross the small positive rotational effect dominating at lower temperatures. The inclusion in Eq.(12) of the first five rotational states of v=1, have numerically confirmed the origin of this weak feature.

In Fig. 9 the Arrehnius plot of the rate constant in the ultra-cold regime is shown. From Fig. 7 we can see that the concavity of the rate as function of T changes sign, so that the rates vary progressively less with the temperature, approaching around a few tens of mK the constant Wigner limit [54]:

$$k_{wig} = \frac{4\pi\beta}{\mu} \tag{17}$$

Using for the imaginary scattering lenghts β the value found in Sec. 3.2 we obtain k_{wig} = 1.789 10^{-12} cm^{-3} molecule^{-1} sec^{-1}, reported in the figure as a dot-dashed line.

The rate constant calculated by Eq.(14) are given in a tabular form in the supplementary material [43] in the full range of temperatures examinated. The accuracy of the numbers supplied, relatively to the PES employed, is estimated to be within 1 %. However, in most of the applications, a more compact analytical fit form is preferred. Most of the astrochemical databases use a Koij/Arrhenius formula to fit the data:

$$k_{Koij}(T) = A(T/300)^B e^{-\frac{C}{T}} \tag{18}$$

In a recent work [55], we have suggested and alternative three terms extension to the Arrhenius equation:

$$k_{dArr}(T) = A(1 - d\frac{\epsilon}{RT})^{\frac{1}{d}} \tag{19}$$

succesfully used to fit the low temperature behaviour of the F + H_2 reaction rates [56]. The results of the fits using Eqs. (18 and 19) are reported in Fig. 7 (the fit parameters are given in the caption). From the comparison, we note that the d-Arrhenius equation of Eq. (19) have a larger range of validity with respect to the fit of Eq. (18) and fit slightly better the data. In the range between 15-2000 K the largest errors are about to 10% around to 60 K. Although the error increase a lot at lower temperatures (around to 30-40 %) the global behaviour is reasonable well described until 1 K. Moreover, the fit have quantitative accuracy above

220 K where the errors are within 1 %. The range of validity of the Koij/Arrhenius fit start around to 30 K with deviations between 5 and 10 % until 200 K, and quickly diverges at lower temperatures. At higher temperatures the fit deviations remain around to 2-3 %. However no one of the two fits employed permit the change of the concavity required to describes the ultra-cold behaviour where finer functional forms are required [57].

4 Final Remarks and Conclusions

In this work, the dynamics of the title reaction has been studied from 1 mK to 2000 K by close coupling quantum reactive scattering calculations [23]. The main tools that have permitted to cover a so large range of temperature varying by six orders of magnitude, have been the implementation of the Enhanced Renormalized Numerov method [25] to improve the convergence in the ultra-cold regime (see Fig. 1) and a massive parallelization of the code [22, 29] to treat the large number of partial waves required for this ionic system (see Sec. 2.1). Integral cross sections have been obtained and compared with previous theoretical [13, 14, 15] and experimental data [18] (see Fig. 2). The comparison has shown relevant differences (about a factor two) for collision energies larger than 200 meV. The analysis indicates that the discrepancies with the previous dynamical calculations are presumably due to the relevance to the Coriolis coupling neglected in previous works. Arguably, the deviations with the measurements of the pioneering experiment [18] come from the calibration of the absolute values. In fact, The quantum mechanical ics obtained in the high collision energy range have shown little sensitivity to the reactant's roto-vibrational energy (see Fig. 3) and preliminary calculations (not shown) with other PESs available for the system (see Sec. 2.2), have confirmed that this result is nearly independent from the details of the PES employed. Otherwise, the ics obtained in the high collision energy range are in reasonable agreement with the simplest capture theory model [44]. As indicated in the previous theoretical calculations, important resonance features appear in the low energy range where the ics show a large maximum around 10 meV. The rich resonance pattern is much more evident in the vibrationally resolved results (see Fig. 5), that also present a change of the main reaction mechanism in the low and high collision energy range, leading to hot and cold vibrational distributions respectively. However, no resonance or virtual states effects have been found below 0.1 meV, where the ics reach smoothly the Wigner regime (see Fig. 6), at variance from previous results [14], demostrating that an 'exact' quantum mechanical treatment of the dynamics is strictly necessary to obtain realistic results in the ultra-cold energy range.

The calculations in the cold regime (below 1 meV) have also shown that the main shape of the excitation functions is independent of the rotational energy of the reactants (see Fig. 4), in disagreement with the conclusions of the previous published calculations [15]. A significant negative rotational effect is found in this collision energy range. However, a good agreement with the previous theoretical data is found for the dynamics restricted to the reactant's ground state. Again, the reason of the disagreement is presumably to be attributed to the larger relevance to the Coriolis coupling in the dynamics of the excited rotational states (see Table I). The good agreement of the ground state dynamics in the cold energy range, leads to a good agreement of the rate constants betwen 5 and 70 K (see Fig. 7 and Table II), a range of temperatures highly relevant in the early universe evolution models. However, the large difference at higher temperatures (see Fig. 8), where the rates are about double in the new time independent calculations, may have important consequences in the early universe scenario. In fact, a higher reactivity of the HeH^+ cation makes the title reaction more competitive with radiative dissociation favouring the formation of the H_2 (see Sec. 1) at higher red shift, where the HeH^+ mechanism is the main channel of formation of the hydrogen molecule [5]. It is highly relevant to date the formation of the first stars and galaxies because the H_2 molecule is at the present state of the astrophysical knowledge [58], the most important coolant species in the early universe scenario. To know exactly how much and in which way the quantum mechanical results here presented affect the evolutionary models requires of course a new determination of the molecular abudances also considering the rapid increases of accurate close coupling data recently available in literature [59, 60] on the others key reactions of the chemical network. We hope that this work will stimulate astrophysical studies in this direction.

Acknowledgements

The Basque Fundation for Science is acknowledged for an Ikerbasque Visiting Fellowship grant in the University of the Basque Country of Leioa (Bilbao) during which most of the work has been done. Prof. D. Sokolovski (Bilbao) is also acknowledged for the warm and friendly hospitality. The author tanks Professors C. Petrongolo (Pisa), S. Cavalli (Perugia), A. Aguado (Madrid) and Dr. F. Esposito (Bari), and L. Bonnet (Bordeaux) for scientific discussions and the Italian MIUR for financial support by PRIN 2010/2011 grant N. 2010ERFKXL. A particular acknowledgment is addressed to Prof. V. Aquilanti (Perugia) for a careful reading of the manuscript and for constant encouragments. Computational time has been supplied by CINECA

(Bologna) under ISCRA project N. HP10CJX3D4.

References

[1] S. Lepp, P.C. Stancil and A. Dalgarno; J. Phys. B: At. Mol. Opt. Phys. **35**, R35 (2002).

[2] M.S. Smith, L.H. Kawano and R.A. Malaney; Astrophys. J. Supp. S. **85**, 219 (1993).

[3] B. Zygelman, P.C. Stancil and A. Dalgarno; Astrophys. J. **508**, 151 (1998).

[4] D. De Fazio, M. de Castro-Vitores, A. Aguado, V. Aquilanti and S. Cavalli; J. Chem. Phys. **137**, 244306 (2012).

[5] C. M. Hirata and N. Padmanabhan; Mon. Not. R. Astron. Soc., **372**, 1175 (2006).

[6] D. Galli and F. Palla; A&A **335**, 403 (1998).

[7] P.S. Julienne; Nature Physics, **8**, 642 (2012).

[8] C. Wellers, A. Borodin, S. Vasilyev, D. Offenberg and S. Schiller; Phys. Chem. Chem. Phys. **13**, 18799 (2011).

[9] G.J. Harris, A.E. Lynas-Gray, S. Miller and J. Tennyson; Astrophys. J. **617**, L143 (2004).

[10] W. Roberge and A. Dalgarno; Astrophys. J. **255**, 489 (1982).

[11] J.J. Lv, X.G. Liu, J.J. Liang and H.Z. Sun; Can.J. Phys. **88**, 899 (2010).

[12] J.J. Liang, X.G. Liu, W.W. Xu, H. Kong and Q.G. Zhang; J. Mol. Struc.-THEOCHEM **942**, 93 (2010).

[13] S. Bovino, M. Tacconi, F.A. Gianturco and D. Galli; A&A **529**, A140 (2011).

[14] S. Bovino, M. Tacconi and F.A. Gianturco; J. Phys. Chem. A **115**, 8197 (2011).

[15] S. Bovino, F.A. Gianturco and M. Tacconi; Chem. Phys. Lett. **554**, 47 (2012).

[16] C. M. Coppola, S. Longo, M. Capitelli, F. Palla and D. Galli; Astrophys. J. Supp. S. **193**, 7 (2011).

[17] Z. Karpas, V. Anicich and W.T. Huntress; J. Chem. Phys. **70**, 2877 (1979).

[18] J.A. Rutherford and D.A. Vroom; J. Chem. Phys. **58**, 4076 (1973).

[19] F. Linder, R.K. Janev and J. Botero; *Atomic and Molecular Processes in Fusion Edge Plasmas*, edited by R.K. Janev (Plenum Press, New York, 1995), p.397.

[20] P.C. Stancil, S. Lepp and A. Dalgarno; Astrophys. J. **509**, 1 (1998).

[21] D.R.G. Schleicher, D. Galli, F. Palla, M. Camenzind, R.S. Klessen, M. Bartelmann and S.C.O. Glover; A&A **490**, 521 (2008).

[22] D. De Fazio, J.M. Lucas, V. Aquilanti and S. Cavalli; Phys Chem. Chem. Phys. **13**, 8571 (2011).

[23] D. Skouteris, J.F. Castillo and D.E. Manolopoulos; Comp. Phys. Comm. **133**, 128 (2000).

[24] D.E. Manolopoulos; J. Chem. Phys. **85**, 6425 (1986).

[25] F.D. Colavecchia, F. Mrugala, G.A. Parker and R. T Pack; J. Chem. Phys. **118**, 10387 (2003).

[26] A. E. Thorlacius and E. D. Cooper; J. Comput. Phys. **72**, 70 (1987).

[27] N. Balakrishnan and A. Dalgarno; Chem. Phys. Lett. **341**, 652 (2001); *Erratum* **351**, 159 (2002).

[28] D. De Fazio, F.A. Gianturco, J.A. Rodriguez-Ruiz, K.T. Tang and J.P. Tonnies; J. Phys. B: At. Mol. Opt. Phys. **27**, 303 (1994).

[29] D. De Fazio and A. Aguilar; in Science and Supercomputing in Europe - report 2011

[30] B.H. Choi, R.T. Poe, J.C. Sun and K.T. Tang; J. Chem. Phys. **78**, 5590 (1983).

[31] S.D. Chao, S.A. Harich, D,X. Dai, C.C. Wang, X. Yang and R.T. Skodje; J. Chem. Phys. **117**, 8341 (2002).

[32] T. Joseph and N. Sathyamurthy; J. Chem. Phys. **86**, 704 (1987).

[33] D.R. Mc Laughlin and D.L. Thompson; J. Chem. Phys. **70**, 2748 (1979).

[34] A. Aguado and M. Paniagua; J. Chem. Phys. **96**, 1265 (1992).

[35] P. Palmieri, C. Puzzarini, V. Aquilanti, G. Capecchi, S. Cavalli, D. De Fazio, A. Aguilar, X. Giménez and J.M. Lucas; Mol. Phys. **98**, 1835 (2000).

[36] T.H. Dunning; J. Chem. Phys. **90**, 1007 (1989).

[37] V. Aquilanti, S. Cavalli and D. De Fazio; J. Chem. Phys. **109**, 3792 (1998).

[38] C.N. Ramachandran, D. De Fazio, S. Cavalli, F. Tarantelli and V. Aquilanti; Chem. Phys. Lett. **469**, 26 (2009).

[39] MOLPRO is a package of *ab initio* programs written by H.-J. Werner and P.J. Knowles, with contributions of J. Almlof, R.D. Amos, M.J.O. Deegan, S.T. Ebert, C.Hampel, W. Meyer, K. Peterson, R.M. Pitzer, A.J. Stone, P.R. Taylor.

[40] S. Wolfram, *The Mathematica book*, 4th Ed., Wolfram Media/Cambridge University Press, 1999.

[41] W. A. Chupka and M. E. Russel; J. Chem. Phys. **49**, 5426 (1968).

[42] X.N. Tang, H. Xu, T. Zhang, Y. Hou, C. Chang, C.Y. Ng, Y. Chiu, R.A. Dressler and D.J. Levandier; J. Chem. Phys. **122**, 164301 (2005).

[43] See Electronic Supplementary Information (ESI) for numerical values of the $H + HeH^+(v=0,j=0)$ total ics and rate constants. A subroutine of the PES used is also included.

[44] G. Gioumousis and D.P. Stevenson; J. Chem. Phys. **29**, 294 (1958).

[45] D. De Fazio and J.F. Castillo; Phys. Chem. Chem. Phys. **1**, 1165 (1999).

[46] T.S. Chu and K.L. Han; Phys. Chem. Chem. Phys. **10**, 2431 (2008).

[47] D. De Fazio, S. Cavalli, V. Aquilanti, A.A. Buchacenko and T.V. Tscherbul; J. Phys. Chem. A **111**, 12538 (2007).

[48] D. Sokolovski, D. De Fazio, S. Cavalli and V. Aquilanti; J. Chem. Phys. **126**, 121101 (2007).

[49] D. Sokolovski, D. De Fazio, S. Cavalli and V. Aquilanti; Phys. Chem. Chem. Phys. **9**, 5664 (2007).

[50] D. De Fazio, V. Aquilanti, S. Cavalli, A. Aguilar and J.M. Lucas; J. Chem. Phys. **129**, 064303 (2008).

[51] T. Kohler, K. Goral and P.S. Julienne; Rev. Mod. Phys. **78**, 1311 (2006).

[52] H.R. Sadeghpour, J.L. Bohn, M.J. Cavagnero, B.D. Esry, I.I. Fabrikant, J.H. Macek and A.R.P. Rau; J. Phys. B: At. Mol. Opt. Phys. **33**, R93 (2000).

[53] N. Balakrishnan, V. Kharchenko, R.C. Forrey and A. Dalgarno; Chem. Phys. Lett. **280**, 5 (1997).

[54] P.F. Weck and N. Balakrishnan; Int. Rev. Phys. Chem. **25**, 83 (2007).

[55] V. Aquilanti, K.C. Mundim, S. Cavalli, D. De Fazio, A. Aguilar and J. M. Lucas; Chem. Phys. **398**, 186 (2012).

[56] V. Aquilanti, S. Cavalli, D. De Fazio, A. Volpi, A. Aguilar and J. M. Lucas; Chem. Phys. **308**, 237 (2005).

[57] S. Cavalli, V. Aquilanti, K.C. Mundim and D. De Fazio; to be published.

[58] D. Galli and F. Palla; Ann. Rev. Astron. Astrophys. **51**, 163 (2013).

[59] T. Gonzalez-Lezana, P. Hounvalt and Y. Scribano; J. Chem. Phys. **139**, 054301 (2013).

[60] L. Pagani, P. Lesaffre, M. Jorfi, P. Hounvalt, T. Gonzalez-Lezana and A. Faure; A&A **551**, A38 (2013).

Table I. Input parameters for the ABC code [23] used in the Production runs. We adopt here the following definitions: maximum value of the Total Angular Momentum ($Jtotmx$) quantum number and of its projection in the body-fixed frame ($kmax$); maximum value of the diatomic rotational states with energy below to $emax$ included in the basis set; maximum value of the hyperradius ($rmax$) and its grid size ($drho$); collision energy grid size (dE).

Collision Energy range (meV)[a,b]	Jtotmx	kmax	emax (eV)[b]	jmax	drho (bohr)	rmax (bohr)	dE (meV)
1 10^{-5}-1.9 10^{-4}	0	0	2.3	22	0.125	40	10^{-5}
2 10^{-4}-2.0 10^{-3}	1	1	2.1	24	0.125	40	10^{-4}
0.003-0.201	3	3	2.1	24	0.125	40	0.001
0.21-2.19	8	4	2.1	24	0.125	30	0.01
			j=1				
0.03-2.02	7	3	2.1	24	0.125	20	0.01
			j=2				
0.06-2.05	8	4	2.1	24	0.125	20	0.01
			j=3				
0.01-2.00	9	5	2.1	24	0.125	20	0.01
2.2-43.8	20	20	2.1	24	0.125	30	0.2
44-244	40	16	2.1	26	0.125	15	1.0
254-604	60	12	2.3	28	0.125	15	10.0
614-1264	79	12	2.5	30	0.125	15	50.0

[a] Total Energy E_{tot} = E_{col} + $E_{v=0}$ + $E_{rot}(j)$; $E_{v=0}$=946.15294 meV, $E_{rot}(j$=1,2 and 3) = 8.313, 24.890 and 49.636 meV.

[b] zero energy in the bottom valley of the products.

Table II. Calculated rate constants (in cm^3 $molecule^{-1}$ s^{-1} $\times$ 10^{-11}) as a function of the temperature, and comparison with Ref. [13].

	Present Result			Ref. [13]
T (K)	j_{max}=0	j_{max}=5	j, v=all	j_{max}=0
0.001	0.1806	0.1806	0.1806	
0.005	0.1834	0.1834	0.1834	
0.01	0.1875	0.1875	0.1875	
0.05	0.2070	0.2070	0.2070	
0.1	0.2312	0.2312	0.2312	
0.5	0.3723	0.3723	0.3723	
1	0.5155	0.5155	0.5155	0.441
5	2.021	2.021	2.021	2.11
10	5.247	5.247	5.247	5.47
20	13.63	13.55	13.55	13.3
30	22.44	22.04	22.04	21.1
50	37.58	36.70	36.70	34.3
70	49.35	48.48	48.48	43.9
80	54.29	53.50	53.50	47.6
100	62.80	62.21	62.21	53.3
200	89.95	90.62	90.62	67.6
300	105.0	107.7	107.7	73.9
500	122.2	128.5	128.9	80.8
800	136.5	145.4	146.4	87.0
1000	143.0	152.4	153.5	
1500	154.3	163.1	163.5	
2000	161.5	168.9	165.2	

Captions to figures

Figure 1. Convergence of the total (summed over all the open roto-vibrational channels of the product) $J = 0$ ics for the H + HeH^+(v=0,j=0) $\rightarrow$ He + H_2^+ reaction as a function of the number of hyperradial points n_{max}. Black filled circles are the results of the quantum mechanical code used and red empty circles are the results of the original ABC code of Ref. [23]. The lines connecting the circles are only a guide to the eye. Three translational collision energies (reported in the panels) in the ultra-cold, cold and low collision energy range are selected. The blue solid line shows the asymptotic values while dot-dashed blue lines delimit the range of ics whithin 1 $\%$ accuracy. The remaining input parameters of the calculations (see Table I for definitions) are set to have a convergence better than 0.1$\%$ ($jmax$, $emax$ and $rmax$ = 30, 2.5 eV and 40 a.u. respectively).

Figure 2. Total ics for the H + HeH^+(v=0,j=0) $\rightarrow$ He + H_2^+ reaction as a function of the translational collision energy. The solid black line is the present time-independent quantum mechanical result, while the dashed violet line is the result digitized from Ref. [13]. Both theoretical results have been obtained using the RMRCI6 PES. The experimental results (filled circles with error bars) have been obtained digitizing the absolute values reported in Fig. 3 of Ref. [18]. Also reported as dotted dashed line is the fit of the experimental results from Ref. [19] and as solid green line the results obtained using the simplest capture model of Ref. [44] (the exact analytical value of 4.5 a.u. was used for the dipole polarizability of the incoming hydrogen atom). Empty circles with dashed error bars are the experiments of Ref. [18] rescaled by 2.358 to match with the theoretical result here presented.

Figure 3. Comparison among theoretical total ics for the H + HeH^+(v=0,j=0,1 and 2) $\rightarrow$ He + H_2^+ reaction. Solid black, red and green lines are time-indipendent quantum mechanical results for reactants rotational state j=0,1 and 2 respectively. Dashed lines are the results obtained digitizing the ics reported in Ref. [15] using the RMRCI6 PES. Possible minor uncertainties could come from the logarithmic scale used for the ics in the latter publication.

Figure 4. Comparison between theoretical total ics for the H + HeH^+(v=0,j=0,1,2 and 3) $\rightarrow$ He + H_2^+ reaction. A logarithmic energy scale is used to emphasize the low energy behaviour. Solid black, red, green and blue lines are quantum mechanical results for reactants rotational state j=0,1,2 and 3 respectively, as indicated in the panels. Dashed lines are the results obtained digitizing the ics reported in Ref. [15].

Figure 5. Vibrationally resolved integral cross sections for the H + HeH^+(v=0,j=0) $\rightarrow$ He + H_2^+(v'=0,1,2 and 3) reaction. A logarithmic energy scale is used to emphasize the low energy behaviour. Black, red, green and blue colours distinguish v'=0,1,2 and 3 product vibrational quantum numbers respectively. Solid and dashed lines are results with and without post-antisymmetrization respectively (see text for details).

Figure 6. Total ics for the H + HeH^+(v=0,j=0) $\rightarrow$ He + H_2^+ reaction as a function of the translational collision energy. A log-log plot is here used to emphasize the ultra-cold behaviour. The solid black line is the present time-independent quantum mechanical result while the dashed violet line is the result digitized from Ref. [14]. Both theoretical results have been obtained using the RMRCI6 PES. The dashed green line is the Wigner's law fit (Eq.(10)) of the ultra-cold ics data, while the dot-dashed black line shows the contribution of J=0 to the ics.

Figure 7. Rate coefficients for the title reaction as a function of the temperature. A log-log plot is here used to emphasize the cold regime. The solid blue line is the result obtained using Eq.(14), while the dashed blue line is the ground state approximation result (Eq.(11 with v, j=0). Filled black circles are the results of Table 2 of Ref. [13], while the filled circle with the error bar is the experimental result of Ref. [17]. All theoretical values have been obtained employing the RMRCI6 PES in the dynamical calculation. The dotted black line is the capture model value obtained by using for dipole polarizzability of the incoming hydrogen atom the exact analytical value of 4.5 a.u. The dot-dashed red and black lines are the results of the fits to the solid line using Eq. (18) (with A = 1.27228 10^{-9}, B = 0.173508 and C = 43.8735) and Eq. (19) (with A = 1.27228 10^{-9}, ϵ = 207.632 and d = - 0.904409 (black line).

Figure 8. The same results of Figure 7 reported on a linear plot to emphasize details in the high temperatures regime. Here, the dot-dashed blue line is the result obtained using Eq.(12) with v_{max}=0 and j_{max}=5.

Figure 9. Ultra-cold behaviour of the rate constants. The dot-dashed line indicates the Wigner limit obtained from the integral cross sections fit of Fig. 6.

Figure 1 De Fazio D

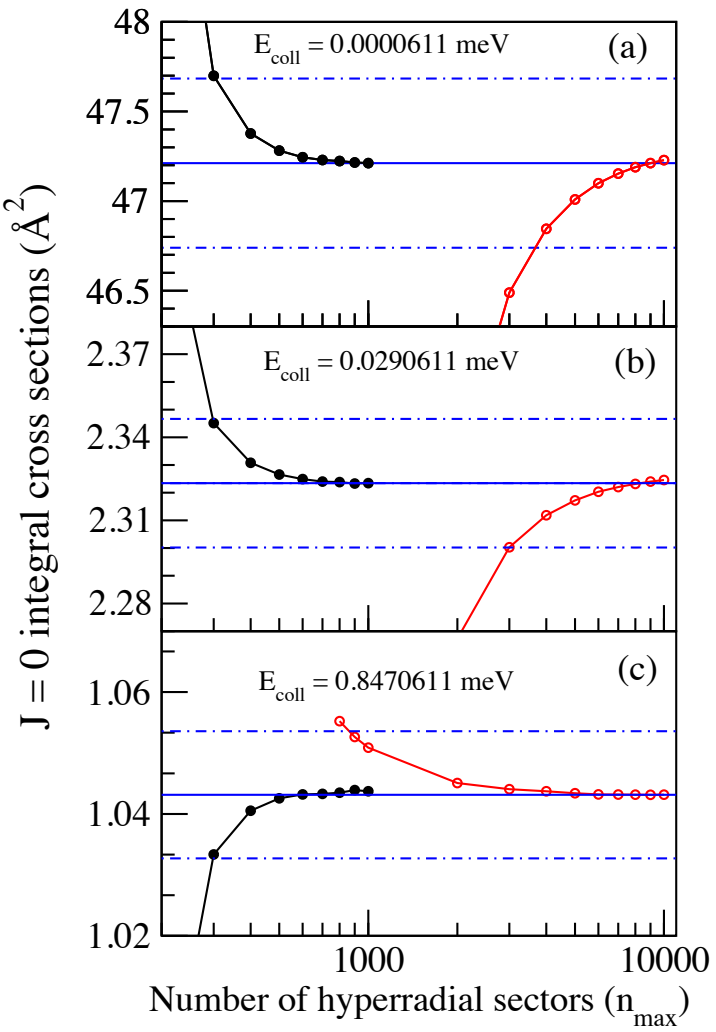

Figure 1:

Figure 2 De Fazio D

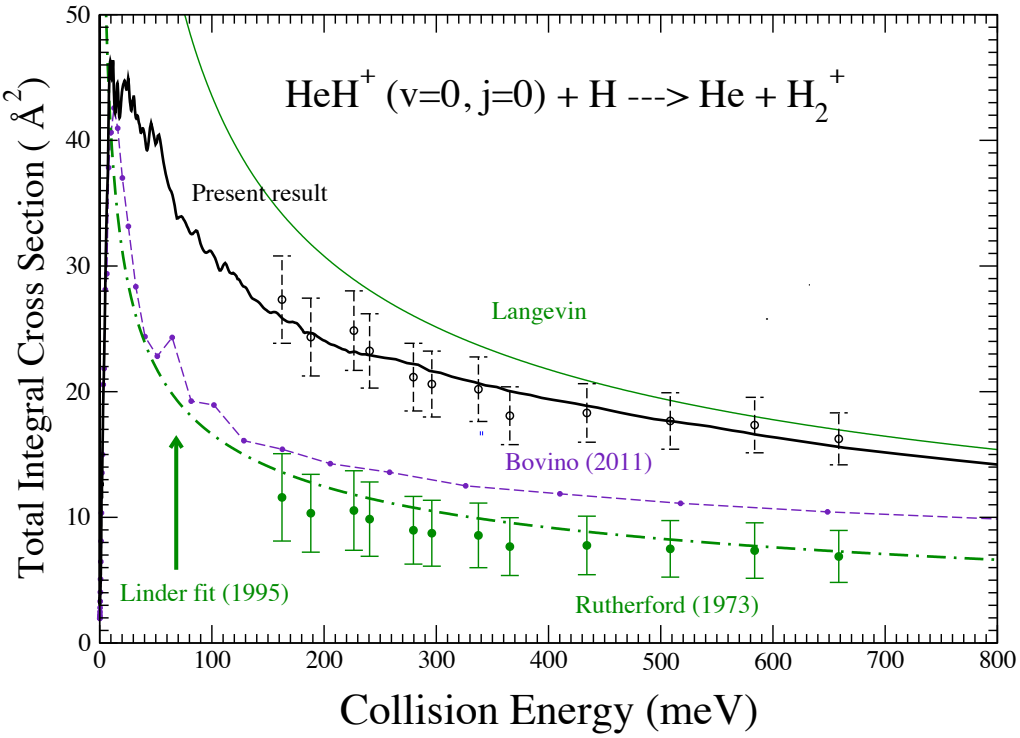

Figure 2:

Figure 3 De Fazio D

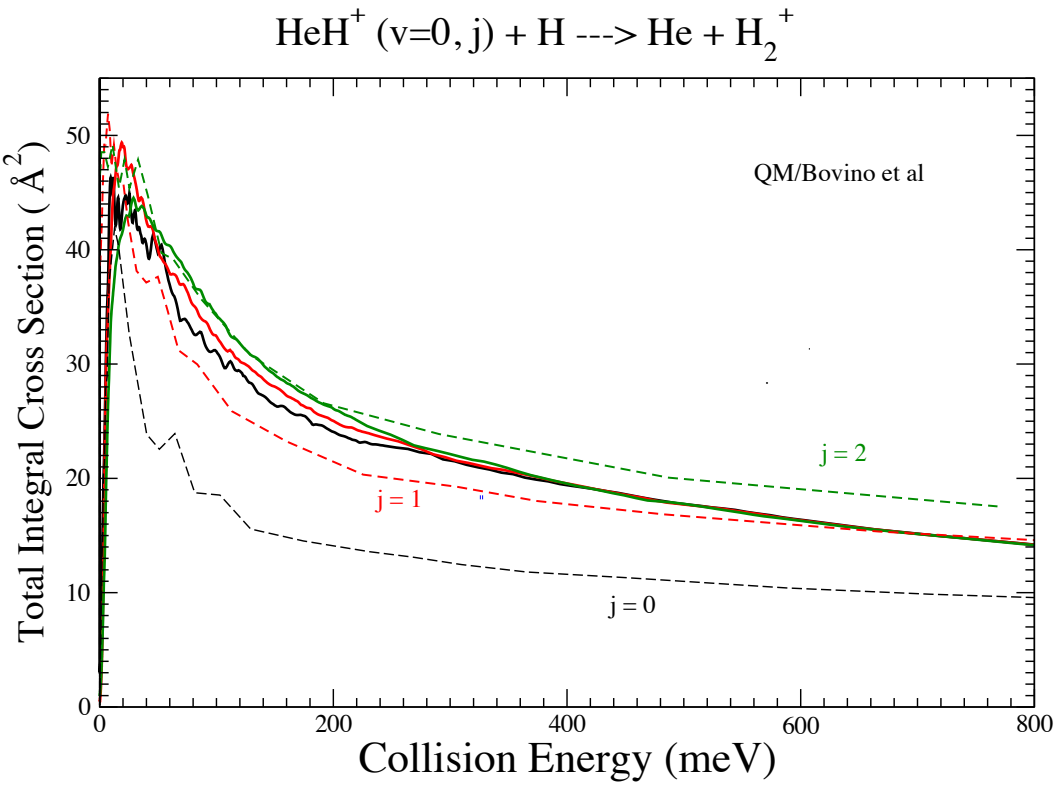

Figure 3:

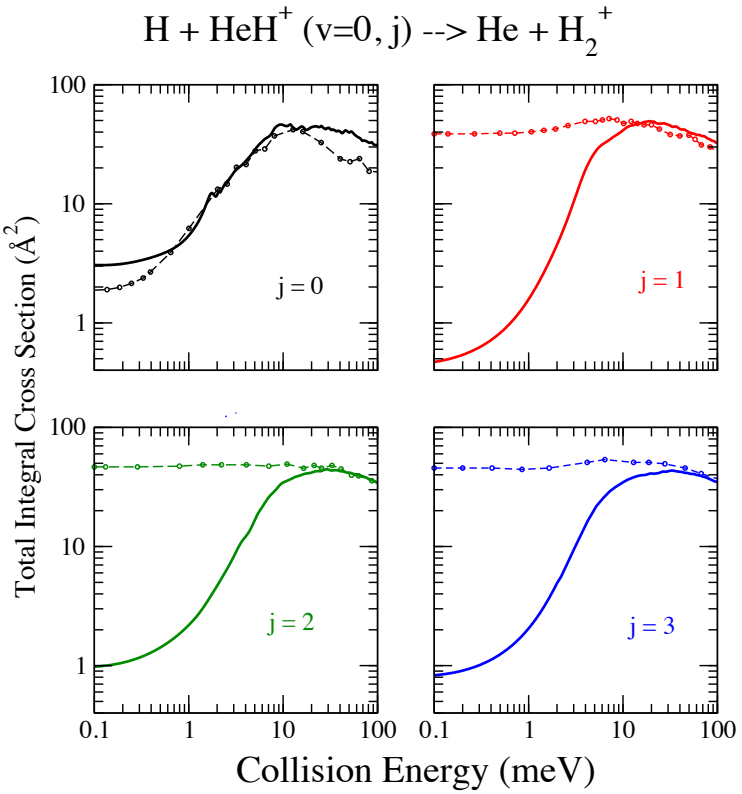

Figure 4 De Fazio D

Figure 4:

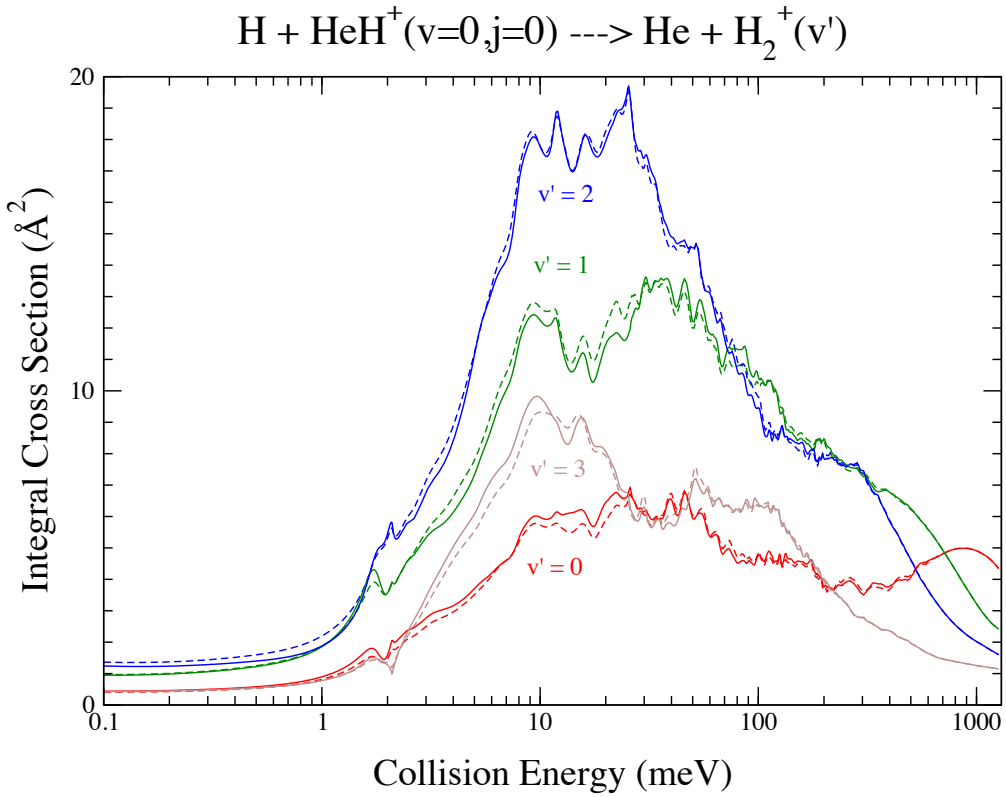

Figure 5 De Fazio D

Figure 5:

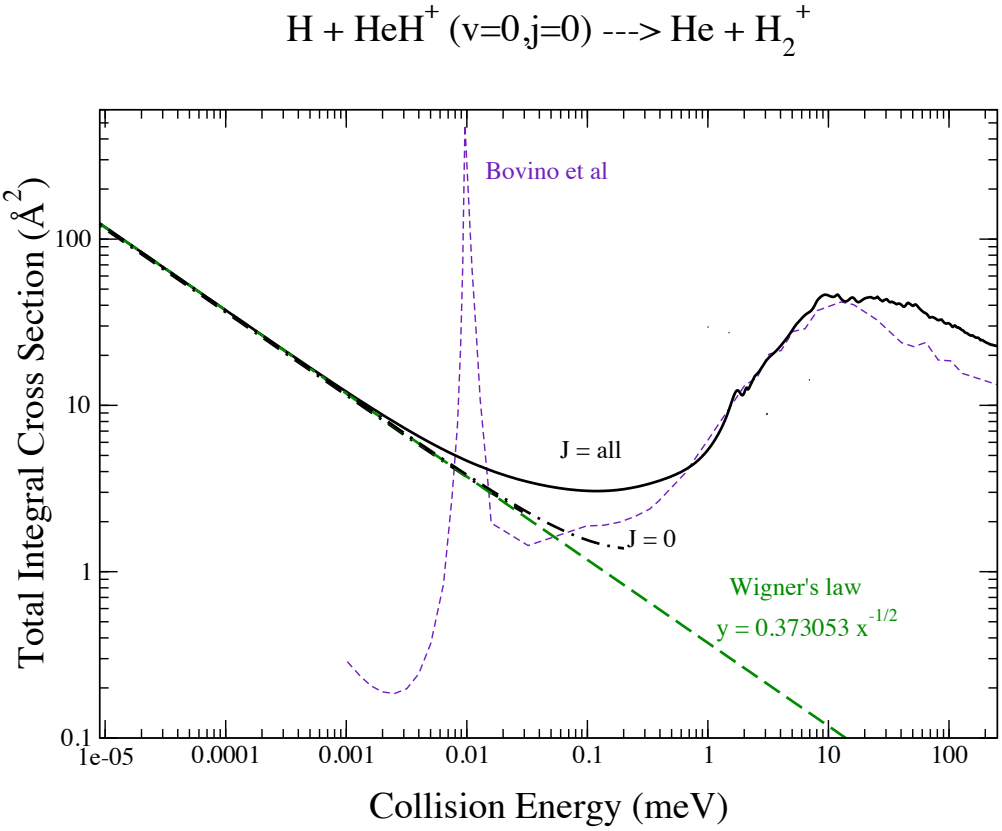

Figure 6 De Fazio D

Figure 6:

Figure 7 De Fazio D

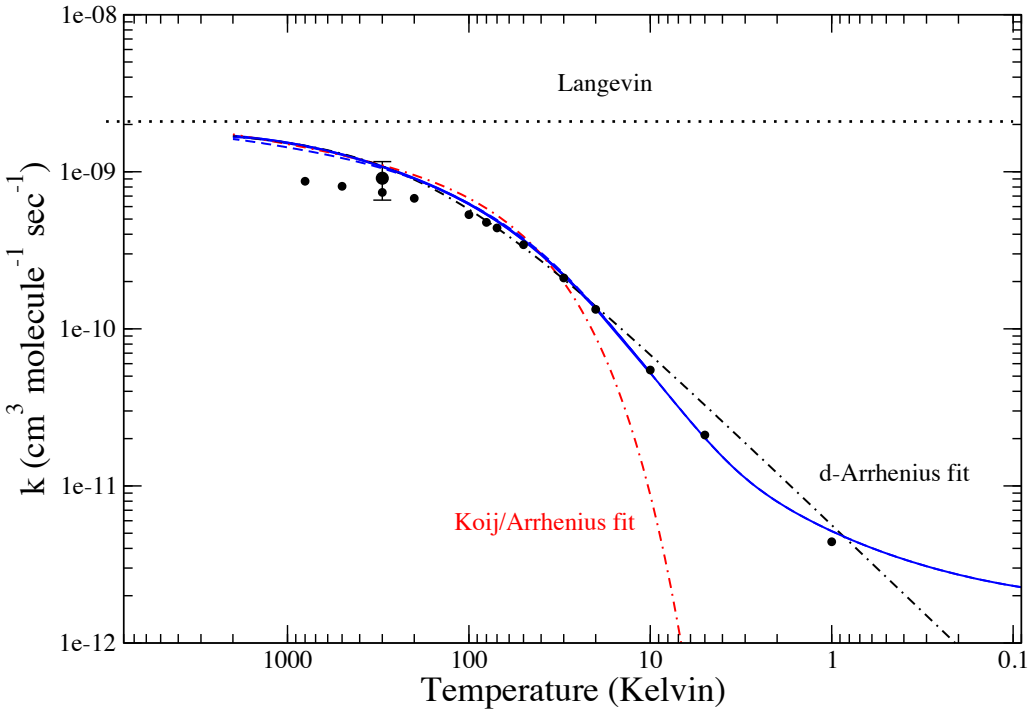

Figure 7:

Figure 8 De Fazio et al

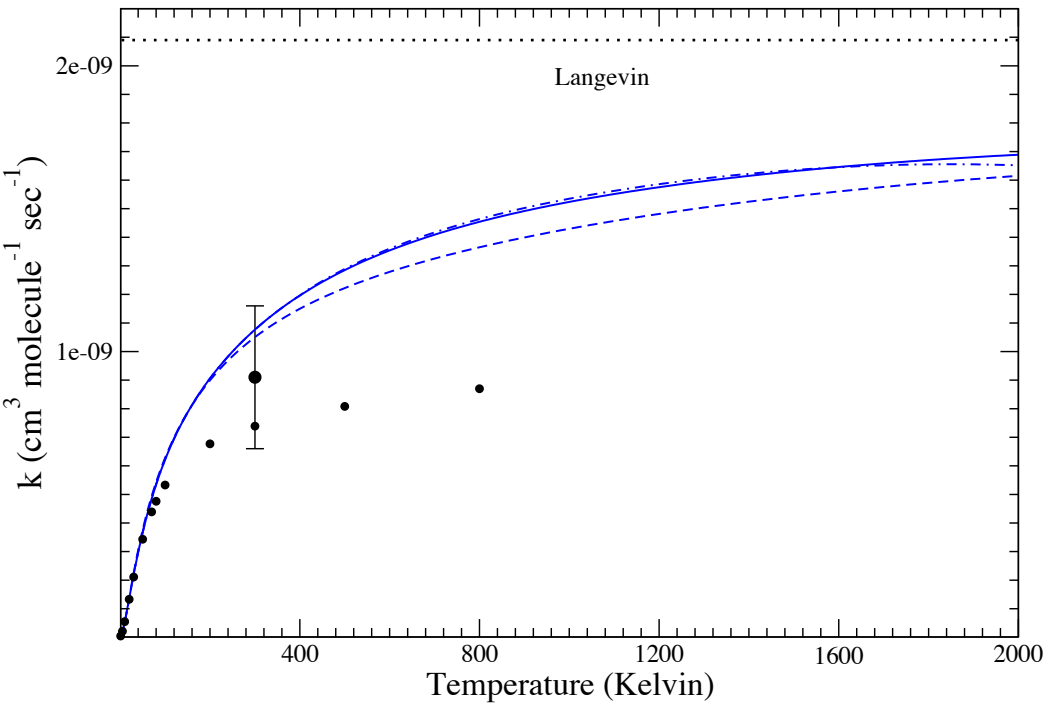

Figure 8:

Figure 9 De Fazio et al

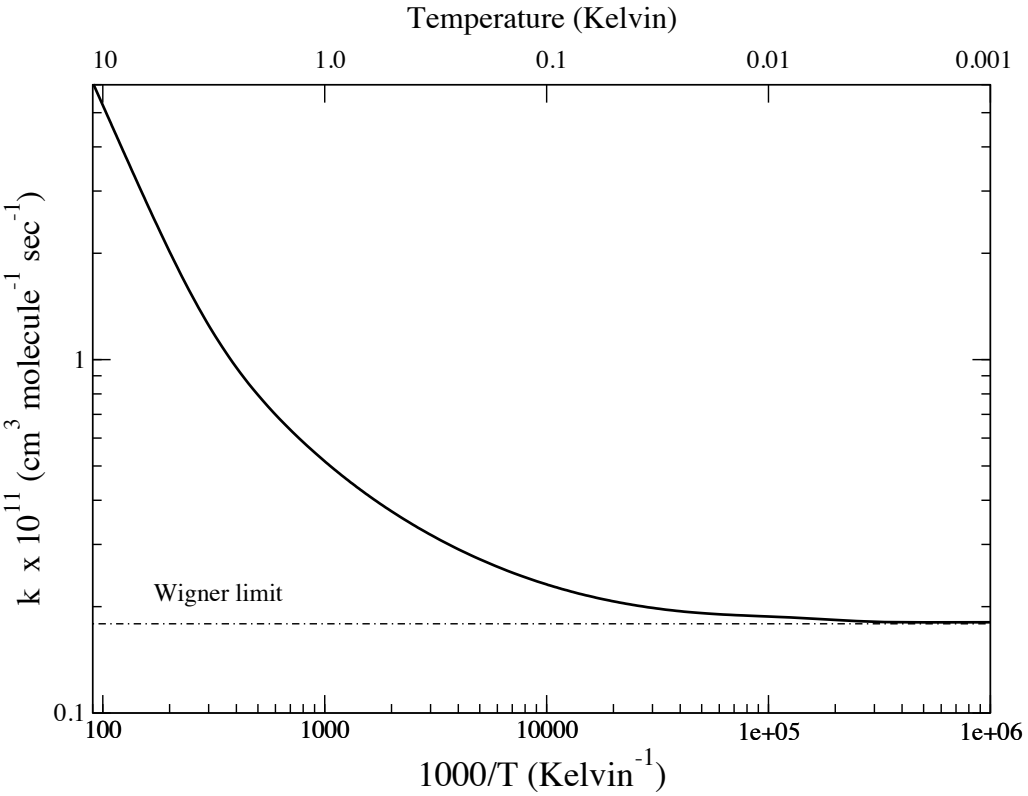

Figure 9: